
Orthogonal Calibration for Asynchronous Federated Learning

Jiayun Zhang
UC San Diego
jiz069@ucsd.edu

Shuheng Li
UC San Diego
shl060@ucsd.edu

Haiyu Huang
UC Los Angeles
haiyu@g.ucla.edu

Xiaofan Yu
UC San Diego
x1yu@ucsd.edu

Rajesh K. Gupta
UC San Diego
rgupta@ucsd.edu

Jingbo Shang
UC San Diego
jshang@ucsd.edu

Abstract

Asynchronous federated learning mitigates the inefficiency of conventional synchronous aggregation by integrating updates as they arrive and adjusting their influence based on staleness. Due to asynchrony and data heterogeneity, learning objectives at the global and local levels are inherently inconsistent—global optimization trajectories may conflict with ongoing local updates. Existing asynchronous methods simply distribute the latest global weights to clients, which can overwrite local progress and cause model drift. In this paper, we propose ORTHOFL, an orthogonal calibration framework that decouples global and local learning progress and adjusts global shifts to minimize interference before merging them into local models. In ORTHOFL, clients and the server maintain separate model weights. Upon receiving an update, the server aggregates it into the global weights via a moving average. For client weights, the server computes the global weight shift accumulated during the client’s delay and removes the components aligned with the direction of the received update. The resulting parameters lie in a subspace orthogonal to the client update and preserve the maximal information from the global progress. The calibrated global shift is then merged into the client weights for further training. Extensive experiments show that ORTHOFL improves accuracy by **9.6%** and achieves a **12×** speedup compared to synchronous methods. Moreover, it consistently outperforms state-of-the-art asynchronous baselines under various delay patterns and heterogeneity scenarios.

1 Introduction

Federated learning [33] is a distributed learning paradigm that allows multiple parties to collaboratively train models without sharing data. The most widely adopted federated learning protocols [33, 28, 21, 27, 46, 59, 58] follow a *synchronous* update procedure, where the server waits for all selected clients to finish local training before aggregating updates. This synchronization becomes inefficient under heterogeneous resource conditions, where clients differ in compute, network bandwidth, and data volume, due to distinct device configurations and user-system interaction patterns.

Asynchronous federated learning offers an alternative approach that aggregates client updates as they arrive (see Figure 1), reducing idle time caused by slower clients. In this setting, when a client is performing local training, the server continuously aggregates updates from other clients, shifting the global model to new states. By the time the client’s update reaches the server, it may be stale.

Existing methods manage such staleness by applying a decay factor to updates before aggregating them into the global model [50, 31, 55, 44]. The updated global model is directly returned to the clients for further training. Although down-weighting a stale update reduces its negative impact on global progress, it also diminishes the integration of meaningful knowledge from the client. Moreover, due to data heterogeneity, the optimization objectives of the global and client models are inherently inconsistent—while the global model aims to optimize for the overall data distribution, individual clients minimize loss on their local data. Distributing the latest global parameters to clients for subsequent training can introduce conflicts with their local optimization steps, potentially reversing local gains and leading to oscillations in training.

To address the challenge, we propose to decouple global and local learning progress and calibrate weight shifts to reduce interference during client weight merging. The key insight is that, in the high-dimensional parameter space of neural networks, there are multiple viable directions for effective optimization [49]. Some of these directions severely disrupt performance on previously learned distributions, while others have little impact. This offers an opportunity to avoid disruptive components in asynchronous updates and preserve both global progress and client-specific contributions.

We introduce ORTHOFL, orthogonal calibration for asynchronous federated learning. Our design is motivated by two goals: (1) minimizing interference between global and local optimization by sharing global information perpendicular to client updates, and (2) selecting the most informative direction within the orthogonal hyperplane to maximize knowledge sharing. Specifically, ORTHOFL maintains separate global and client model weights to accommodate their distinct optimization objectives. When the server receives a client update, the global weights are updated via a moving average with an adaptive decay factor accounting for staleness. For the client model, ORTHOFL identifies the global weight shift (induced by other clients) during the client’s delay. It projects this shift onto the direction of the received client update and subtracts this projected component. The remaining parameters lie in a subspace orthogonal to the client update. Through analysis, we show that this orthogonal calibration strategy keeps maximal global progress while minimizing interference with the local update. The calibrated global shift is then merged with the client model for further training.

For evaluation, we incorporate realistic delay distributions to reflect the heterogeneous nature of real-world deployments. ORTHOFL demonstrates an average of 9.6% accuracy improvement across datasets from diverse application scenarios compared to synchronous methods and a $12\times$ speedup in reaching a target accuracy. Moreover, it outperforms state-of-the-art asynchronous baselines. We also explore various simulated delay distributions and data heterogeneity levels to understand their impact on model performance and convergence speed. In summary, our contributions are as follows:

- We analyze the key challenges of asynchronous federated learning—the inconsistency of global and local objectives and the detrimental effect of stale updates in heterogeneous environments.
- We propose a novel orthogonal calibration method that maintains separate global and local model weights. It projects global shifts onto orthogonal subspaces of local updates before sharing them with clients. This approach reduces interference, preserves meaningful contributions from both global progress and local updates, and enhances knowledge sharing.
- We demonstrate the effectiveness and robustness of ORTHOFL through comprehensive experiments on multiple datasets and various delay scenarios, providing insights on practical design considerations for large-scale federated learning systems.

2 Preliminaries

2.1 Asynchronous System Architecture

In an asynchronous federated learning setup, a central server coordinates the training of a global model W using data distributed across M clients. Each client $m \in \{1, 2, \dots, M\}$ possesses its own

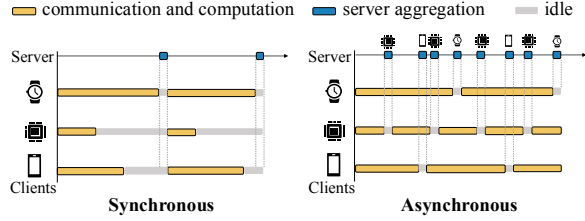


Figure 1: Time synchrony in federated learning. Asynchronous methods reduce idle time and improve resource utilization, suited for large-scale deployments.

local dataset \mathbf{D}_m . The data distribution of client m is denoted as \mathcal{P}_m . The objective is to train a global model W that generalizes well across the combined data distribution of all clients. Formally, we aim to solve the following optimization problem:

$$W^* = \arg \min_W \frac{1}{M} \sum_{m=1}^M \mathbb{E}_{(x,y) \sim \mathcal{P}_m} \ell(f(x; W), y), \quad (1)$$

where W denotes the global weights, ℓ the loss function, and $f(x; W)$ the prediction of the model on data x with model weights W .

Clients perform local training and communicate their updates to the central server at different times. Let T be the number of global rounds. For $t \in \{1, \dots, T\}$, denote $m_t \in \{1, \dots, M\}$ as the client that communicates with the server at the t -th round, and τ_t as the round when client m_t last communicated with the server. We define the staleness of the client update as follows:

Definition 1 (Staleness). *Staleness quantifies the delay between a client’s updates, representing the number of global rounds since the client last communicated with the server. Formally, let t be the current global round, and τ_t the global round when the server last received updates from client m_t . The staleness of client m_t is defined as $t - \tau_t$, where $t - \tau_t \geq 1$. A staleness of 1 indicates no delay.*

For simplicity, we will drop the subscripts on m_t and τ_t with no ambiguity from now on.

2.2 A Motivating Study

We conduct an experiment on MNIST [8] with a LeNet5 [25] model to analyze the challenges in asynchronous federated learning. We simulate the scenario with two clients: one with a 10-second latency and the other with 30, 60, or 100 seconds. We adopt the asynchronous method, FedAsync [50], where client updates are aggregated with decay factors based on latency. Let $W^{(t)}$ denote the global weights at t -th round before aggregation, and $W^{(t+)}$ the global weights after aggregation. Similarly, let $W_m^{(t)}$ represent the model weights of client m at t -th round. The aggregation follows:

$$\beta_t = (t - \tau)^{-a} \cdot \beta, \quad (2)$$

$$W^{(t+)} = (1 - \beta_t)W^{(t)} + \beta_t W_m^{(t)} \quad (3)$$

where β and a are hyperparameters set to $\beta = 0.6$ and $a = 0.5$ as reported in FedAsync. To create non-IID data, each client is assigned a non-overlapping half of the MNIST classes.

The global performance is shown in Figure 2(a), where markers represent updates from the “slow” client with longer latency. We observe an increase in accuracy when the server aggregates updates from the slow client, as these updates introduce knowledge of previously undertrained classes. However, this gain is gradually lost, with accuracy declining to around 0.5 after several updates from the faster client. This suggests the fast client’s updates override the contributions of the slower client. Moreover, as the latency of the slower client increases, the decay factor β_t for integrating its updates decreases. This weakens its contribution to the global model and slows convergence, especially under non-IID data, as valuable knowledge from the slower client is not fully utilized.

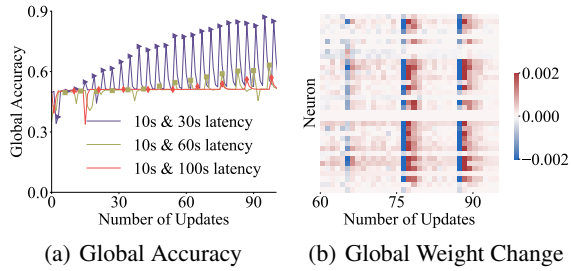


Figure 2: Asynchronous learning with a fast client (10s latency) and a slow client (30/60/100s) assigned non-overlapping classes. Due to objective inconsistency: (a) accuracy spikes when the slow client updates, followed by drops as the fast client updates; (b) update directions shift abruptly when the active client switches.

Figure 2(b) visualizes changes in global model weights in the final hidden layer before the classifier in the case where the latency of the two clients is 10 and 100 seconds respectively. The y-axis represents neurons, and the x-axis represents the number of updates. The color indicates the direction and degree of global weight changes, with red representing an increase and blue a decrease. We observe abrupt

shifts occur when switching between clients. Updates from the slow client often decrease the neuron weights (blue), while subsequent updates from the fast client increase the weight values (red), pulling the model in opposite directions. The antagonistic behavior is due to objective inconsistency—while the global model optimizes for the overall distribution, client updates follow distinct local objectives, driving oscillations in weight aggregation.

3 Method: Orthogonal Weight Calibration

3.1 ORTHOFL Algorithm

Once receiving a client update, ORTHOFL immediately integrates it into the global model. ORTHOFL maintains *separate* variables for global and client models. Before merging global weight shift to the client model, the server orthogonalizes the global shift against the received client update. This orthogonality allows the client to incorporate global progress while continuing its local optimization without disruption. The pseudo-code is presented in Appendix E.

Global Aggregation via Moving Average. Denote $W^{(t)}$ as the global model weights at the t -th round before client update and $W^{(t+)}$ after update. Similarly, let $W_m^{(t)}$ be the client m 's local model weights at the t -th round before update and $W_m^{(t+)}$ after update. Note that $W^{(t+1)} := W^{(t+)}$ as the global model weights stay unchanged after communication with a client before the next client update. We update the global model with a moving average:

$$W^{(t+)} = (1 - \beta_t)W^{(t)} + \beta_t W_m^{(t)}, \quad (4)$$

where β_t controls the contribution of client m 's current update to the aggregation. We let $\beta_t := s_a(t - \tau) \cdot \beta$ with $\beta \in (0, 1)$ and $s_a(x) = x^{-a}$ for some $a > 0$ so that update with a larger staleness has a smaller contribution, and thereby decreasing the influence of client update with long delay.

Calibration on Client Updates. To minimize interference caused by asynchronous updates, we orthogonalize the global weight change that occurs between the client's successive updates against client's local update before sending it to the client for the next round of training. Formally, when the server receives an update from client m , if the staleness $t - \tau > 1$, it calculates the local weight change from its last update to its current update:

$$\Delta W_m = W_m^{(t)} - W_m^{(\tau+)}. \quad (5)$$

Similarly, the server calculates the global weight shift due to aggregating updates from other clients during this period:

$$\Delta W = W^{(t)} - W^{(\tau+)}. \quad (6)$$

To update client m with global progress, the server computes the orthogonal component of ΔW with respect to ΔW_m . The orthogonalization is done for the weight of each layer through removing the component that is parallel to ΔW_m . Let ΔW^l and ΔW_m^l be the change in the layer l of the global weights and the local weights respectively. The component of ΔW^l orthogonal to ΔW_m^l is:

$$\Delta W^{l\perp} = \Delta W^l - \text{proj}_{\Delta W_m^l}(\Delta W^l) = \Delta W^l - \frac{\Delta W^l \cdot \Delta W_m^l}{\Delta W_m^l \cdot \Delta W_m^l} \Delta W_m^l. \quad (7)$$

Let ΔW^\perp represent the aggregation of $\Delta W^{l\perp}$ across all layers. This orthogonal component ΔW^\perp ensures that the updates from the other clients during delay $t - \tau$ do not interfere with the client's local progress, as it removes any component of the global weight change during delay along the direction of the local update. ΔW^\perp is then sent to current client m to form the new client model weight for the subsequent round of local training on client m :

$$W_m^{(t+)} = W_m^{(t)} + \Delta W^\perp. \quad (8)$$

3.2 Mathematical Basis of Orthogonalization

A gradient update orthogonal to previously accumulated gradients helps preserve existing model behavior and minimizes unintended changes to its outputs [12]. Due to the high-dimensional

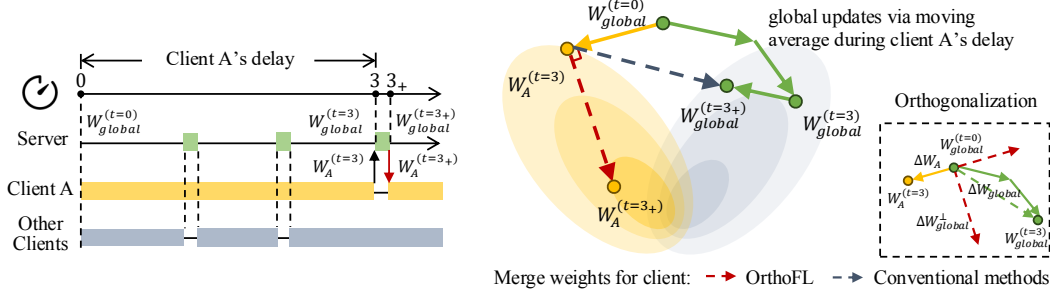


Figure 3: An example of optimization trajectories. Shaded regions represent iso-loss contours for client A (yellow) and other clients (gray). Deeper colors indicate lower loss areas. ORTHOFL removes conflicting components via orthogonalization, merging updates with minimal interference.

parameter space of neural networks, there are multiple directions that are orthogonal to the stale local weight update. We have the following lemma showing that the orthogonalization strategy in ORTHOFL preserves the maximal information from the global weight shift vectors perpendicular to the local update direction. The proof is given in Appendix A.

For $v, w \in \mathbb{R}^d$, let $\langle v, w \rangle := \sum_{i=1}^d v_i w_i$ be the standard inner product on \mathbb{R}^d .

Lemma 3.1. *Let $v \in \mathbb{R}^d$ and $\mathcal{U} = \{u_1, \dots, u_k\}$ be an orthonormal set for some $k < d$. Then for any $w \in (\text{span } \mathcal{U})^\perp$,*

$$\|v - v^\perp\| \leq \|v - w\|, \quad (9)$$

where $v^\perp := v - \sum_{i=1}^k \langle v, u_i \rangle u_i$ denote the component of v orthogonal to \mathcal{U} . Moreover, the angle between v and v^\perp is less than any angle between v and w for $w \in (\text{span } \mathcal{U})^\perp$.

We apply this lemma in our case when $v = \Delta W^l$ and $\mathcal{U} = \{\Delta W_m^l\}$. It implies $\Delta W^{l\perp}$ in equation (7) is the unique vector among those perpendicular to ΔW_m^l with the smallest magnitude of $\|\Delta W^l - \Delta W^{l\perp}\|$ and the smallest angle with ΔW^l . This allows the server to pass the maximum knowledge from global progress to client m without interfering with its most recent update.

3.3 Visualization of Optimization Trajectories

We illustrate the advantage of our method by visualizing an example of optimization trajectories. As shown in Figure 3, client A begins local training from the global state $W_{\text{global}}^{(t=0)}$. Before A's update arrives, the server aggregates two updates from other clients into the global model. Consequently, just before aggregating A's update at $t = 3$, the global model has evolved to $W_{\text{global}}^{(t=3)}$. Meanwhile, client A finishes local training and submits the updated parameters $W_A^{(t=3)}$. The shaded regions show the iso-loss contours for client A (yellow) and the collective optimization space of other clients (gray).

The global weight is updated via a moving average and becomes $W_{\text{global}}^{(t=3+)}$. In conventional asynchronous methods, this global weight is directly assigned to client A (gray dashed line). This would push the model farther from A's optimization objective than $W_A^{(t=3)}$, reversing A's learning progress. ORTHOFL mitigates this by removing the component of the global weight shift that is parallel to ΔW_A . This ensures that the calibrated parameters are orthogonal to A's update direction. Finally, the calibrated global shift is merged into A's model (red dashed line), which becomes $W_A^{(t=3+)}$. This way, ORTHOFL reduces interference due to staleness and objective inconsistencies while preserving meaningful contributions at both global and local levels.

4 Experiments

4.1 Experiment Setup

Compared Methods. We consider baselines including synchronous methods, FedAvg [33], FedProx [28], FedAdam [38], semi-asynchronous methods, FedBuff [36] and CA²FL [47], and fully-

asynchronous methods, FedAsync [50]. The detailed descriptions of these compared methods are provided in Appendix B.2.

Applications and Datasets. Table 1 summarizes the setups for each dataset. We conduct experiments on five datasets, CIFAR-10 and CIFAR-100 [23], MNIST [8], 20 Newsgroups [24], and HAR [2], including three distinct data types: image, text, and time series. To assess the robustness of ORTHOFL across different model architectures, we pair each dataset with a model suited to its data type. To evaluate ORTHOFL’s performance in parameter-efficient fine-tuning (PEFT) settings [15], we employ a pretrained DistilBERT [41] from Hugging Face¹ for evaluations on the 20 Newsgroups dataset and fine-tune it using Low-Rank Adaptation (LoRA) [18], which reduces the number of trainable parameters. More details are given in Appendix B.1.

Table 1: Datasets and models in the experiments.

Datasets	Clients	Avg. $ D_m $	Model	Data Type
CIFAR-10	10	4000	VGG11	image
MNIST	10	6000	LeNet5	image
20 Newsgroups	20	566	DistilBERT	text
HAR	21	350	ResNet18	time-series
CIFAR-100	100	400	MobileNetV2	image

Data Heterogeneity. For the HAR dataset, clients are naturally divided based on the individual subjects, as each subject represents a client. For the other datasets, we set the number of clients equal to the number of classes in each dataset. To create non-IID client distributions, we follow prior work [17] and use a Dirichlet distribution $Dir(\alpha = 0.1)$ to derive class distribution.

Delay Simulation. To ensure controlled evaluation and avoid variability in federated learning deployments, we simulate client delays using measurements (including communication and computational latency) from prior work [54], which were collected using Raspberry Pi (RPI) devices in different home environments with wireless connectivity. To account for differences in the size of models and datasets, we use an RPI 4B which has comparable computational capabilities as the reported ones to measure latency for training one round under each model and dataset configuration. Each configuration is tested five times to derive the average training time. The computational latency for datasets in our experiment is then adjusted based on the ratio between our measured time and the computation latency in [54]. Similarly, communication latency was scaled based on the model size in bytes compared to the model used in the original delay collection. Using these measurements, we calculate the mean and variance of latency for every device. During simulations, we assign the statistics to clients randomly and sample latency for each round from a Gaussian distribution parameterized by the assigned statistics. For fair comparisons, the order of client updates is kept consistent with a fixed set of random seeds across compared methods. Besides these real-world measurements, we also investigate model performance under additional delay distributions in Section 4.5.

Evaluation Metrics. We report accuracy after training for sufficient clock cycles to ensure the method reaches stable performance. For a fair comparison, we fix the same training time across all methods. In addition, we compare the time spent in reaching a target accuracy—set as the 95% of the lowest final accuracy among all compared methods. FedAvg serves as the baseline of time consumption (i.e., $1\times$), and we report the relative time for other methods.

4.2 Main Experiment Results

Table 2 summarizes the results. ORTHOFL consistently outperforms the compared methods across all datasets—it not only converges faster but also achieves higher accuracy. Notably, the advantage becomes more obvious in the setting with a larger number of clients, as seen in CIFAR-100. This is because, for synchronous methods, the client sampling rate decreases as the number of clients increases (e.g., only 10 out of 100 clients are sampled per round), leading to longer wait times and slower convergence. Similarly, for baseline asynchronous methods, although their aggregation mechanisms are designed to mitigate the influence of model staleness, they fail to effectively address the challenges posed by data heterogeneity. In contrast, the calibration mechanism in ORTHOFL alleviates the negative impact of both stale model updates and the model divergence caused by data heterogeneity, ensuring faster convergence and improved performance.

Furthermore, as shown in Figure 4, ORTHOFL demonstrates reduced fluctuations in accuracy over training time. These fluctuations, observed in compared methods, are caused by conflicting updates from clients with non-identical data distributions.

¹<https://huggingface.co/distilbert/distilbert-base-uncased>

Table 2: Main results (%) including average accuracy, standard deviation, and time relative to FedAvg. ORTHOFL reaches the target accuracy more quickly and achieves higher accuracy.

Methods	MNIST		CIFAR-10		20 Newsgroups		HAR		CIFAR-100	
	Accuracy	Time	Accuracy	Time	Accuracy	Time	Accuracy	Time	Accuracy	Time
FedAvg [33]	92.2±1.1	1×	73.8±2.4	1×	58.1±3.1	1×	84.2±0.6	1×	22.2±0.4	1×
FedProx [28]	90.5±0.9	1.09×	73.3±2.2	0.90×	58.6±3.1	0.98×	84.0±0.9	0.98×	20.4±0.6	1.18×
FedAdam [38]	93.8±2.3	0.91×	<u>74.6±1.5</u>	0.78×	58.9±1.8	1.08×	87.1±3.3	0.68×	42.1±1.0	0.36×
FedAsync [50]	95.4±0.7	0.39×	74.3±1.1	<u>0.48×</u>	61.8±3.8	0.27×	87.6±1.9	<u>0.26×</u>	47.9±0.9	0.20×
FedBuff [36]	93.6±2.1	0.46×	73.6±3.2	0.55×	62.1±2.0	0.34×	87.4±1.0	<u>0.30×</u>	<u>62.3±0.5</u>	0.12×
CA ² FL [47]	<u>96.1±1.4</u>	<u>0.30×</u>	69.7±8.0	0.60×	<u>65.7±1.6</u>	<u>0.24×</u>	<u>87.8±1.9</u>	0.29×	61.1±0.7	<u>0.09×</u>
OrthoFL (ours)	98.2±0.3	0.18×	76.5±3.3	0.19×	66.2±1.3	0.09×	89.7±1.0	0.23×	63.0±0.6	0.03×

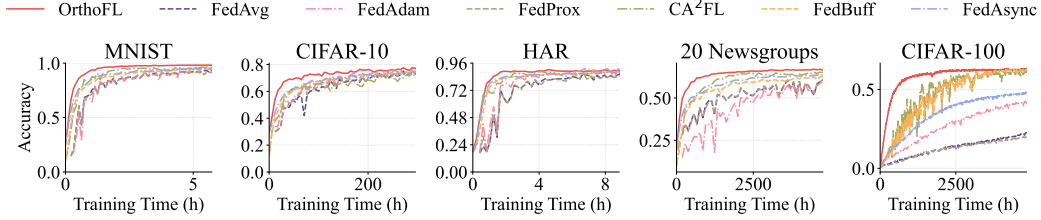


Figure 4: Accuracy w.r.t. training time.

4.3 Overhead Analysis

Compared to baseline methods, ORTHOFL does not introduce additional communication overhead. The extra computational overhead occurs on the server during the orthogonalization process.

The overhead of orthogonal aggregation depends on the model size, as orthogonalization is performed through matrix operations on the weight changes of each layer. As shown in Table 3, the orthogonalization operation in our experiments takes between 3 ms (for MNIST) and 512 ms (for CIFAR-100) when running aggregation on a server equipped with an AMD EPYC 7713 64-Core Processor (3.72 GHz max clock) and 3.9 TiB RAM. This additional time for weight aggregation is negligible compared to the computational and communication latency on clients (shown in Figure 9).

Table 3: Aggregation time of ORTHOFL.

Dataset	Model	Train Params	Time
MNIST	LeNet5	44K	0.003s
HAR	ResNet18	119K	0.199s
20 Newsgroups	DistilBERT	753K	0.110s
CIFAR-10	VGG11	9.2M	0.188s
CIFAR-100	MobileNetV2	2.4M	0.512s

4.4 Ablation Studies

We conduct ablation studies to evaluate our key design choices. First, we set FedAsync as a baseline (denoted as ORTHOFL w/o Calib.), since it can be viewed as our ablation without calibration. Second, we assess the contribution of global aggregation by removing the moving average and directly loading the calibrated client weight into the global model (denoted as ORTHOFL w/o MA). Furthermore, we investigate an alternative orthogonalization strategy that projects the incoming client update onto the orthogonal subspace of the most recent updates from all other clients, (denoted as ORTHOFL-Pairwise Proj.). The orthogonality is achieved through the same process (i.e., removing parallel components) as in ORTHOFL.

We observe performance decreases when clients and the global model share the same weights (ORTHOFLL w/o Calib. and ORTHOFLL w/o MA). ORTHOFLL w/o MA performs particularly poorly as the absence of a global moving average causes overfitting to individual client distributions. These results emphasize the need to decouple global and local learning to address objective inconsistencies. Furthermore, ORTHOFLL-pairwise Proj. achieves performance comparable to ORTHOFLL, suggesting that effective orthogonal calibration can be realized through multiple viable ways. We expect that fine-tuning the orthogonalization strategy could further bring improvement to the model performance and we leave such exploration for future work.

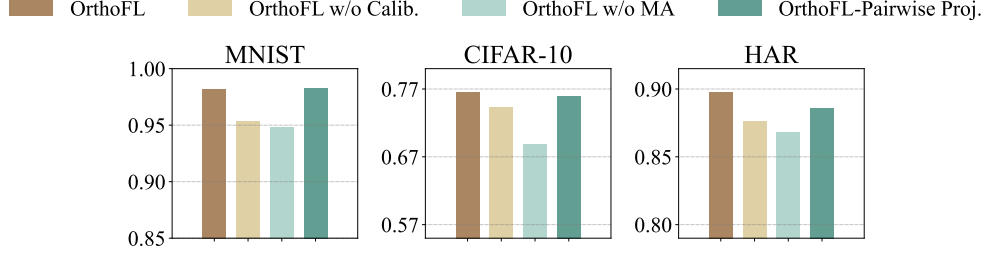


Figure 5: Ablation study. The results emphasize the importance of decoupling global and local learning to address objective inconsistencies. Besides, effective orthogonal calibration can be achieved via multiple viable approaches.

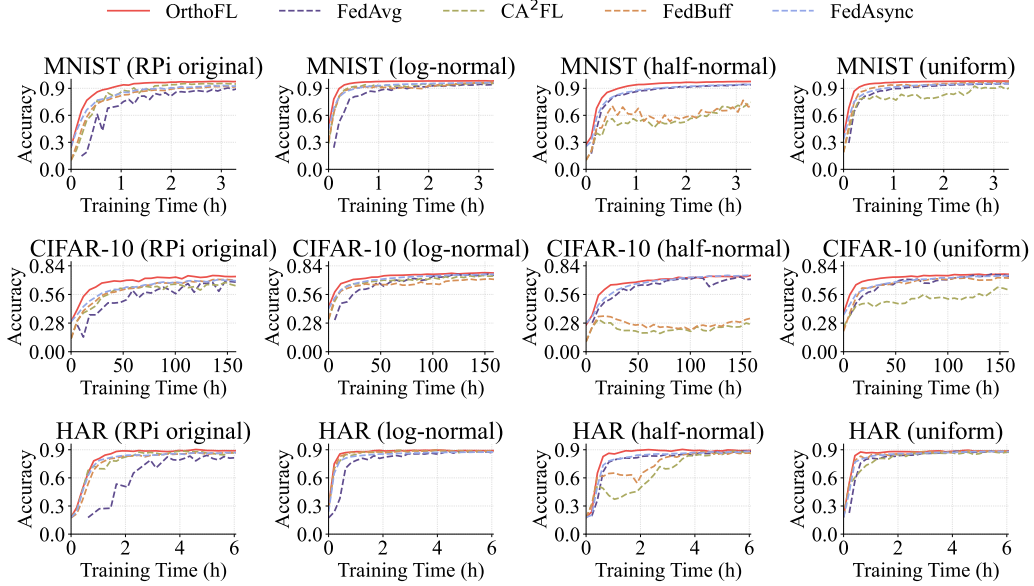


Figure 6: Performance with different delay distributions.

4.5 Exploratory Studies

How do algorithms perform under different delay distributions? Since real-world deployment of federated learning may present diverse delay patterns, we explore other possible delay distributions in real-world setups, such as following log-normal, half-normal [45], and uniform distributions [36].

Each distribution is parameterized by the mean and variance of latency (communication and computation) observed across the RPi devices. Details on deriving these distributions are provided in Appendix B.4. Figure 6 presents the accuracy curves for each algorithm under different delay distributions. With real-world measured RPi latency, some clients experience substantially longer latencies, causing synchronous methods like FedAvg to converge more slowly as the server waits for stragglers. In this case, asynchronous methods generally have better performance than synchronous ones. Under the lognormal, half-normal, and uniform delay distributions, extreme latencies are less common, so the performance gap between synchronous and asynchronous methods narrows. However, the two buffer-based semi-asynchronous methods are sensitive to the delay patterns as they show lower performance under half-normal and uniform latency. In general, ORTHOFL performs the best across all scenarios, demonstrating its robustness against different delay patterns.

How does data heterogeneity impact performance? To control the level of data heterogeneity, we change α for Dirichlet distribution from $\{0.01, 0.1, 0.5, 10^4\}$, where $\alpha = 10^4$ simulates the IID case. We present experiments on MNIST and CIFAR-10 as shown in Figure 7. As the client data distribution becomes more heterogeneous (i.e., lower values of α), we observe the performance of

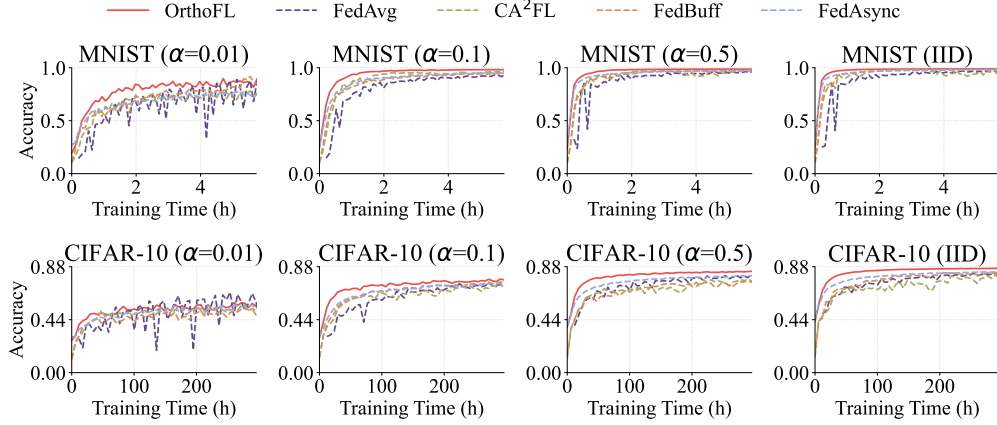


Figure 7: Performance under different data heterogeneity levels.

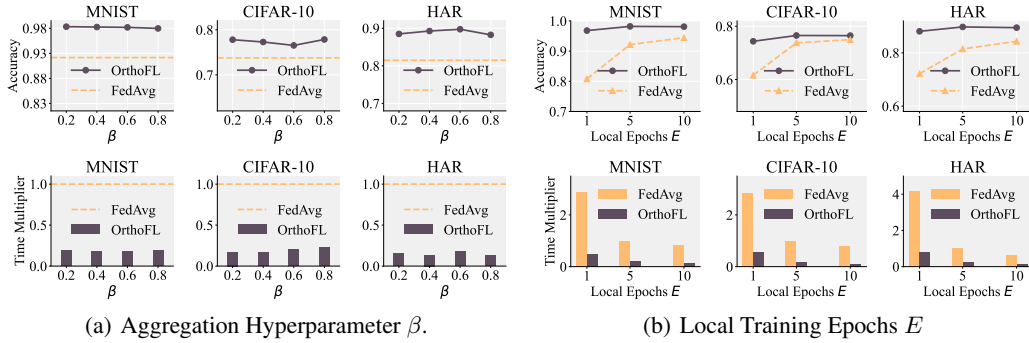


Figure 8: Sensitivity analysis. (a) ORTHOFL is robust to aggregation hyperparameter β , maintaining higher accuracy than FedAvg and a low relative time. (b) An appropriately chosen number of local epochs E improves accuracy within the same training duration and expedites convergence.

baseline methods has more fluctuations and decreases in final accuracy. This is because client models trained on non-IID data distributions have larger divergences in their weights. Aggregating divergent updates amplifies inconsistencies, leading to slower convergence and lower accuracy for baseline methods. By contrast, ORTHOFL exhibit stable performance across all settings. In the IID case, where data is uniformly distributed across clients, ORTHOFL still outperforms the compared methods. This is because our orthogonal calibration also addresses model staleness.

4.6 Sensitivity Analyses

Aggregation Hyperparameter. The parameter β in Equation 4 acts as a smoothing factor that balances the contribution of client updates to the global model and the retention of the global model’s weights from the previous round. A larger β allows the global model to incorporate more of the client updates, potentially accelerating learning, while a smaller β preserves more of the global model’s previous state, enhancing stability. We vary the value of β from $\{0.2, 0.4, 0.6, 0.8\}$. As shown in Figure 8(a), ORTHOFL is robust to different β values and always achieves higher accuracy than FedAvg after a fixed training time, and the relative time of ORTHOFL is low.

Number of Local Training Epochs. The number of local training epochs E determines how much information is learned during a round and impacts the overall convergence speed. A larger E allows clients to learn more information from their local data, potentially improving local model performance. However, it has the risk of larger divergence among client models and global models. On the other hand, setting a smaller E ensures closer alignment between client and global models but comes at the cost of higher communication latency due to more frequent synchronization. We vary the value of E from $\{1, 5, 10\}$ and show the results in Figure 8(b). The upper row shows the final accuracy

after a fixed training time and the bottom row presents the relative time to reach 95% of FedAvg’s target accuracy when $E = 5$. We observe that when $E = 1$, both methods reach lower accuracy compared to larger E . This is due to insufficient local learning, requiring more communication rounds to achieve comparable performance. ORTHOFL achieves similar final accuracy when $E = 5$ and $E = 10$. Notably, ORTHOFL outperforms FedAvg across different E values. The speedup of ORTHOFL is more obvious at smaller E values (e.g., $E = 1$).

5 Related Works

We review two core directions relevant to our study. Connections with other areas including asynchronous stochastic gradient descent and continual learning are discussed in Appendix C.

Federated Learning and Heterogeneity Problem. Federated learning [33] is a distributed learning paradigm that allows multiple parties to jointly train machine learning models without data sharing, preserving data privacy. Despite the potential, it faces significant challenges due to heterogeneity among participating clients, which is typically classified into two main categories: data heterogeneity and system heterogeneity. Data heterogeneity appears as clients own non-IID (independent and identically distributed) data [28, 21, 46, 59]. The difference in data distribution causes the local updates to deviate from the global objective, making the aggregation of these models drift from the global optimum and deteriorating convergence. System heterogeneity refers to variations in client device capabilities, such as computational power, network bandwidth, and availability [46, 57, 26, 11, 1, 58]. These disparities lead to uneven progress among clients, and the overall training process is delayed by slow devices. Traditional federated learning approaches rely on synchronization for weight aggregation [33, 28, 38], where the server waits for all clients selected in a round to complete and return model updates before proceeding with aggregation. This synchronization leads to inefficient resource utilization and extended training times, particularly in large-scale deployments involving hundreds or thousands of clients. Addressing the heterogeneity issues is a critical problem for improving the scalability and efficiency of federated learning systems in real-world deployment.

Asynchronous Federated Learning. Much of the asynchronous federated learning literature focuses on staleness management by assigning weights for aggregating updates according to factors including delay in updates [50], divergence from the global model [44, 55] and local losses [31]. For example, [50] lets the server aggregate client updates into the global model with a weight determined by staleness. Another line of research caches client updates at the server and reuses them to calibrate global updates [13, 47]. For example, [47] maintains the latest update for every client to estimate their contribution to the current aggregation and calibrate global updates. Furthermore, semi-asynchronous methods [36, 55] balance between efficiency and training stability. For example, [36] buffers a fixed number of client updates before aggregation. We select representative methods from each category for our comparisons. Besides, some works improve efficiency from a different perspective—through enhanced parallelization. Methods include decoupling local computation and communication [3] and parallelizing server-client computation [56]. In addition, asynchronous architectures have been explored in other paradigms such as vertical [60] and clustered [30] federated learning. While these directions complement our work, they fall outside the scope of this study.

6 Conclusions

In this paper, we introduce ORTHOFL, an orthogonal calibration mechanism for asynchronous federated learning. ORTHOFL exploits the high-dimensional parameter space of neural networks and projects the global weight shift during a client’s delay onto a subspace orthogonal to its stale update. This projection ensures global progress is integrated into client models without disrupting local learning. Experiments demonstrate that ORTHOFL consistently outperforms state-of-the-art synchronous and asynchronous baselines, achieving notable gains in accuracy, convergence speed, and robustness under diverse delay patterns and data heterogeneity.

For future work, we plan to explore more complicated scenarios such as dynamic client participation and failure tolerance. Discussions on the adaptability of ORTHOFL to these challenges are provided in Appendix D. We also aim to further optimize learning efficiency, potentially through integrating adaptive client selection into ORTHOFL to prioritize impactful clients for participation. These explorations will further enhance the robustness and scalability of federated learning.

References

- [1] Samiul Alam, Luyang Liu, Ming Yan, and Mi Zhang. 2022. FedRolex: Model-Heterogeneous Federated Learning with Rolling Sub-Model Extraction. *Advances in Neural Information Processing Systems* 35 (2022), 29677–29690.
- [2] Davide Anguita, Alessandro Ghio, Luca Oneto, Xavier Parra, Jorge Luis Reyes-Ortiz, et al. 2013. A public domain dataset for human activity recognition using smartphones.. In *Esann*, Vol. 3. 3.
- [3] Dmitrii Avdiukhin and Shiva Kasiviswanathan. 2021. Federated learning under arbitrary communication patterns. In *International Conference on Machine Learning*. PMLR, 425–435.
- [4] Rotem Zamir Aviv, Ido Hakimi, Assaf Schuster, and Kfir Y Levy. 2021. Learning under delayed feedback: Implicitly adapting to gradient delays. *arXiv preprint arXiv:2106.12261* (2021).
- [5] Arslan Chaudhry, Naeemullah Khan, Puneet Dokania, and Philip Torr. 2020. Continual learning in low-rank orthogonal subspaces. *Advances in Neural Information Processing Systems* 33 (2020), 9900–9911.
- [6] Cheng Chen, Ji Zhang, Jingkuan Song, and Lianli Gao. 2022. Class gradient projection for continual learning. In *Proceedings of the 30th ACM International Conference on Multimedia*. 5575–5583.
- [7] Alon Cohen, Amit Daniely, Yoel Drori, Tomer Koren, and Mariano Schain. 2021. Asynchronous stochastic optimization robust to arbitrary delays. *Advances in Neural Information Processing Systems* 34 (2021), 9024–9035.
- [8] Li Deng. 2012. The mnist database of handwritten digit images for machine learning research. *IEEE Signal Processing Magazine* 29, 6 (2012), 141–142.
- [9] Jiahua Dong, Lixu Wang, Zhen Fang, Gan Sun, Shichao Xu, Xiao Wang, and Qi Zhu. 2022. Federated class-incremental learning. In *Proceedings of the IEEE/CVF conference on computer vision and pattern recognition*. 10164–10173.
- [10] Sanghamitra Dutta, Gauri Joshi, Soumyadip Ghosh, Parijat Dube, and Priya Nagpurkar. 2018. Slow and stale gradients can win the race: Error-runtime trade-offs in distributed SGD. In *International conference on artificial intelligence and statistics*. PMLR, 803–812.
- [11] Xiuwen Fang and Mang Ye. 2022. Robust Federated Learning with Noisy and Heterogeneous Clients. In *Proceedings of the IEEE/CVF Conference on Computer Vision and Pattern Recognition*. 10072–10081.
- [12] Mehrdad Farajtabar, Navid Azizan, Alex Mott, and Ang Li. 2020. Orthogonal gradient descent for continual learning. In *International Conference on Artificial Intelligence and Statistics*. PMLR, 3762–3773.
- [13] Xinran Gu, Kaixuan Huang, Jingzhao Zhang, and Longbo Huang. 2021. Fast federated learning in the presence of arbitrary device unavailability. *Advances in Neural Information Processing Systems* 34 (2021), 12052–12064.
- [14] Saurabh Gupta, Tirthak Patel, Christian Engelmann, and Devesh Tiwari. 2017. Failures in large scale systems: long-term measurement, analysis, and implications. In *Proceedings of the International Conference for High Performance Computing, Networking, Storage and Analysis*. 1–12.
- [15] Zeyu Han, Chao Gao, Jinyang Liu, Jeff Zhang, and Sai Qian Zhang. 2024. Parameter-efficient fine-tuning for large models: A comprehensive survey. *arXiv preprint arXiv:2403.14608* (2024).
- [16] Kaiming He, Xiangyu Zhang, Shaoqing Ren, and Jian Sun. 2016. Deep residual learning for image recognition. In *CVPR*. 770–778.
- [17] Tzu-Ming Harry Hsu, Hang Qi, and Matthew Brown. 2019. Measuring the Effects of Non-Identical Data Distribution for Federated Visual Classification. *arXiv preprint arXiv:1909.06335* (2019).

- [18] Edward J Hu, Yelong Shen, Phillip Wallis, Zeyuan Allen-Zhu, Yuanzhi Li, Shean Wang, Lu Wang, and Weizhu Chen. 2021. Lora: Low-rank adaptation of large language models. *arXiv preprint arXiv:2106.09685* (2021).
- [19] Insu Jang, Zhenning Yang, Zhen Zhang, Xin Jin, and Mosharaf Chowdhury. 2023. Oobleck: Resilient distributed training of large models using pipeline templates. In *Proceedings of the 29th Symposium on Operating Systems Principles*. 382–395.
- [20] Myeongjae Jeon, Shivaram Venkataraman, Amar Phanishayee, Junjie Qian, Wencong Xiao, and Fan Yang. 2019. Analysis of Large-Scale Multi-Tenant GPU clusters for DNN training workloads. In *2019 USENIX Annual Technical Conference (USENIX ATC 19)*. 947–960.
- [21] Sai Praneeth Karimireddy, Satyen Kale, Mehryar Mohri, Sashank Reddi, Sebastian Stich, and Ananda Theertha Suresh. 2020. SCAFFOLD: Stochastic Controlled Averaging for Federated Learning. In *ICML*. PMLR, 5132–5143.
- [22] Anastasiia Koloskova, Sebastian U Stich, and Martin Jaggi. 2022. Sharper convergence guarantees for asynchronous SGD for distributed and federated learning. *Advances in Neural Information Processing Systems* 35 (2022), 17202–17215.
- [23] Alex Krizhevsky, Geoffrey Hinton, et al. 2009. Learning multiple layers of features from tiny images. (2009).
- [24] Ken Lang. 1995. Newsweeder: Learning to filter netnews. In *Machine learning proceedings 1995*. Elsevier, 331–339.
- [25] Yann LeCun, Léon Bottou, Yoshua Bengio, and Patrick Haffner. 1998. Gradient-based learning applied to document recognition. *Proc. IEEE* 86, 11 (1998), 2278–2324.
- [26] Ang Li, Jingwei Sun, Xiao Zeng, Mi Zhang, Hai Li, and Yiran Chen. 2021. FedMask: Joint Computation and Communication-Efficient Personalized Federated Learning via Heterogeneous Masking. In *Proceedings of the 19th ACM Conference on Embedded Networked Sensor Systems*. 42–55.
- [27] Qinbin Li, Bingsheng He, and Dawn Song. 2021. Model-contrastive federated learning. In *Proceedings of the IEEE/CVF conference on computer vision and pattern recognition*. 10713–10722.
- [28] Tian Li, Anit Kumar Sahu, Manzil Zaheer, Maziar Sanjabi, Ameet Talwalkar, and Virginia Smith. 2020. Federated Optimization in Heterogeneous Networks. *MLSys* 2 (2020), 429–450.
- [29] Sen Lin, Li Yang, Deliang Fan, and Junshan Zhang. 2022. Trgp: Trust region gradient projection for continual learning. *arXiv preprint arXiv:2202.02931* (2022).
- [30] Boyi Liu, Yiming Ma, Zimu Zhou, Yexuan Shi, Shuyuan Li, and Yongxin Tong. 2024. CASA: Clustered Federated Learning with Asynchronous Clients. In *Proceedings of the 30th ACM SIGKDD Conference on Knowledge Discovery and Data Mining*. 1851–1862.
- [31] Ji Liu, Juncheng Jia, Tianshi Che, Chao Huo, Jiayang Ren, Yang Zhou, Huaiyu Dai, and Dejing Dou. 2024. Fedasmu: Efficient asynchronous federated learning with dynamic staleness-aware model update. In *Proceedings of the AAAI Conference on Artificial Intelligence*, Vol. 38. 13900–13908.
- [32] Yuhang Ma, Zhongle Xie, Jue Wang, Ke Chen, and Lidan Shou. 2022. Continual Federated Learning Based on Knowledge Distillation.. In *IJCAI*. 2182–2188.
- [33] Brendan McMahan, Eider Moore, Daniel Ramage, Seth Hampson, and Blaise Aguera y Arcas. 2017. Communication-efficient learning of deep networks from decentralized data. In *Artificial intelligence and statistics*. PMLR, 1273–1282.
- [34] Konstantin Mishchenko, Francis Bach, Mathieu Even, and Blake E Woodworth. 2022. Asynchronous SGD beats minibatch SGD under arbitrary delays. *Advances in Neural Information Processing Systems* 35 (2022), 420–433.

- [35] Konstantin Mishchenko, Franck Iutzeler, Jérôme Malick, and Massih-Reza Amini. 2018. A delay-tolerant proximal-gradient algorithm for distributed learning. In *International conference on machine learning*. PMLR, 3587–3595.
- [36] John Nguyen, Kshitiz Malik, Hongyuan Zhan, Ashkan Yousefpour, Mike Rabbat, Mani Malek, and Dzmitry Huba. 2022. Federated learning with buffered asynchronous aggregation. In *International Conference on Artificial Intelligence and Statistics*. PMLR, 3581–3607.
- [37] Tae Jin Park, Kenichi Kumatani, and Dimitrios Dimitriadis. 2021. Tackling dynamics in federated incremental learning with variational embedding rehearsal. *arXiv preprint arXiv:2110.09695* (2021).
- [38] Sashank Reddi, Zachary Charles, Manzil Zaheer, Zachary Garrett, Keith Rush, Jakub Konečný, Sanjiv Kumar, and H Brendan McMahan. 2020. Adaptive federated optimization. *arXiv preprint arXiv:2003.00295* (2020).
- [39] Gobinda Saha, Isha Garg, and Kaushik Roy. 2021. Gradient projection memory for continual learning. *arXiv preprint arXiv:2103.09762* (2021).
- [40] Mark Sandler, Andrew Howard, Menglong Zhu, Andrey Zhmoginov, and Liang-Chieh Chen. 2018. Mobilenetv2: Inverted residuals and linear bottlenecks. In *Proceedings of the IEEE conference on computer vision and pattern recognition*. 4510–4520.
- [41] V Sanh. 2019. DistilBERT, A Distilled Version of BERT: Smaller, Faster, Cheaper and Lighter. *arXiv preprint arXiv:1910.01108* (2019).
- [42] Karen Simonyan and Andrew Zisserman. 2014. Very deep convolutional networks for large-scale image recognition. *arXiv preprint arXiv:1409.1556* (2014).
- [43] Sebastian U Stich and Sai Praneeth Karimireddy. 2019. The error-feedback framework: Better rates for SGD with delayed gradients and compressed communication. *arXiv preprint arXiv:1909.05350* (2019).
- [44] Ningxin Su and Baochun Li. 2022. How asynchronous can federated learning be?. In *2022 IEEE/ACM 30th International Symposium on Quality of Service (IWQoS)*. IEEE, 1–11.
- [45] Kaixin Sui, Mengyu Zhou, Dapeng Liu, Minghua Ma, Dan Pei, Youjian Zhao, Zimu Li, and Thomas Moscibroda. 2016. Characterizing and improving wifi latency in large-scale operational networks. In *MobiSys*. 347–360.
- [46] Jianyu Wang, Qinghua Liu, Hao Liang, Gauri Joshi, and H. Vincent Poor. 2020. Tackling the Objective Inconsistency Problem in Heterogeneous Federated Optimization. *NeurIPS* 33 (2020), 7611–7623.
- [47] Yujia Wang, Yuanpu Cao, Jingcheng Wu, Ruoyu Chen, and Jinghui Chen. 2024. Tackling the Data Heterogeneity in Asynchronous Federated Learning with Cached Update Calibration. In *International Conference on Learning Representations*.
- [48] Qizhen Weng, Wencong Xiao, Yinghao Yu, Wei Wang, Cheng Wang, Jian He, Yong Li, Liping Zhang, Wei Lin, and Yu Ding. 2022. MLaaS in the wild: Workload analysis and scheduling in Large-Scale heterogeneous GPU clusters. In *19th USENIX Symposium on Networked Systems Design and Implementation (NSDI 22)*. 945–960.
- [49] Mitchell Wortsman, Maxwell C Horton, Carlos Guestrin, Ali Farhadi, and Mohammad Rastegari. 2021. Learning neural network subspaces. In *International Conference on Machine Learning*. PMLR, 11217–11227.
- [50] Cong Xie, Sanmi Koyejo, and Indranil Gupta. 2019. Asynchronous federated optimization. *arXiv preprint arXiv:1903.03934* (2019).
- [51] Cong Xie, Sanmi Koyejo, and Indranil Gupta. 2020. Zeno++: Robust fully asynchronous SGD. In *International Conference on Machine Learning*. PMLR, 10495–10503.

- [52] Xin Yang, Hao Yu, Xin Gao, Hao Wang, Junbo Zhang, and Tianrui Li. 2024. Federated continual learning via knowledge fusion: A survey. *IEEE Transactions on Knowledge and Data Engineering* (2024).
- [53] Jaehong Yoon, Wonyong Jeong, Giwoong Lee, Eunho Yang, and Sung Ju Hwang. 2021. Federated continual learning with weighted inter-client transfer. In *International Conference on Machine Learning*. PMLR, 12073–12086.
- [54] Xiaofan Yu, Lucy Cherkasova, Harsh Vardhan, Quanling Zhao, Emily Ekaireb, Xiyuan Zhang, Arya Mazumdar, and Tajana Rosing. 2023. Async-HFL: Efficient and robust asynchronous federated learning in hierarchical IoT networks. In *Proceedings of the 8th ACM/IEEE Conference on Internet of Things Design and Implementation*. 236–248.
- [55] Yu Zang, Zhe Xue, Shilong Ou, Lingyang Chu, Junping Du, and Yunfei Long. 2024. Efficient Asynchronous Federated Learning with Prospective Momentum Aggregation and Fine-Grained Correction. In *Proceedings of the AAAI Conference on Artificial Intelligence*, Vol. 38. 16642–16650.
- [56] Feilong Zhang, Xianming Liu, Shiyi Lin, Gang Wu, Xiong Zhou, Junjun Jiang, and Xiangyang Ji. 2023. No one idles: Efficient heterogeneous federated learning with parallel edge and server computation. In *International Conference on Machine Learning*. PMLR, 41399–41413.
- [57] Jie Zhang, Song Guo, Xiaosong Ma, Haozhao Wang, Wenchao Xu, and Feijie Wu. 2021. Parameterized Knowledge Transfer for Personalized Federated Learning. *Advances in Neural Information Processing Systems* 34 (2021), 10092–10104.
- [58] Jiayun Zhang, Shuheng Li, Haiyu Huang, Zihan Wang, Xiaohan Fu, Dezhi Hong, Rajesh K Gupta, and Jingbo Shang. 2024. How Few Davids Improve One Goliath: Federated Learning in Resource-Skewed Edge Computing Environments. In *Proceedings of the ACM on Web Conference 2024*. 2976–2985.
- [59] Jiayun Zhang, Xiyuan Zhang, Xinyang Zhang, Dezhi Hong, Rajesh K Gupta, and Jingbo Shang. 2023. Navigating Alignment for Non-identical Client Class Sets: A Label Name-Anchored Federated Learning Framework. In *Proceedings of the 29th ACM SIGKDD Conference on Knowledge Discovery and Data Mining*. 3297–3308.
- [60] Ke Zhang, Ganyu Wang, Han Li, Yulong Wang, Hong Chen, and Bin Gu. 2024. Asynchronous Vertical Federated Learning for Kernelized AUC Maximization. In *Proceedings of the 30th ACM SIGKDD Conference on Knowledge Discovery and Data Mining*. 4244–4255.
- [61] Shuxin Zheng, Qi Meng, Taifeng Wang, Wei Chen, Nenghai Yu, Zhi-Ming Ma, and Tie-Yan Liu. 2017. Asynchronous stochastic gradient descent with delay compensation. In *International Conference on Machine Learning*. PMLR, 4120–4129.

A Proof

In this section, we present the proof for Lemma 3.1. We restate the lemma below:

Lemma A.1. *Let $v \in \mathbb{R}^d$ and $\mathcal{U} = \{u_1, \dots, u_k\}$ be an orthonormal set for some $k < d$. Then for any $w \in (\text{span } \mathcal{U})^\perp$,*

$$\|v - v^\perp\| \leq \|v - w\|, \quad (10)$$

where $v^\perp := v - \sum_{i=1}^k \langle v, u_i \rangle u_i$ denote the component of v orthogonal to \mathcal{U} . Moreover, the angle between v and v^\perp is less than any angle between v and w for $w \in (\text{span } \mathcal{U})^\perp$.

Proof. Extend \mathcal{U} to an orthonormal basis $\mathcal{B} := \{u_1, \dots, u_k, u_{k+1}, \dots, u_d\}$ on \mathbb{R}^d . Write $w = \sum_{i=1}^d w_i u_i$ and $v = \sum_{i=1}^d v_i u_i$, where $w_i := \langle w, u_i \rangle$ and $v_i := \langle v, u_i \rangle$ denote the coordinates of w and v with respect to the basis \mathcal{B} respectively. Since $w \in (\text{span } \mathcal{U})^\perp$, $w_i = 0$ for $1 \leq i \leq k$. It follows from Pythagorean theorem that

$$\begin{aligned} \|v - w\|^2 &= \left\| \sum_{i=1}^d (v_i - w_i) u_i \right\|^2 \\ &= \left\| \sum_{i=1}^k v_i u_i + \sum_{j=k+1}^d (v_j - w_j) u_j \right\|^2 \\ &= \left\| \sum_{i=1}^k v_i u_i \right\|^2 + \left\| \sum_{j=k+1}^d (v_j - w_j) u_j \right\|^2 \\ &\geq \left\| \sum_{i=1}^k v_i u_i \right\|^2. \end{aligned} \quad (11)$$

Taking square root of both sides and noting that by definition $v - v^\perp = \sum_{i=1}^k v_i u_i$, equation (10) follows. As for the second claim, let $\theta(v, w)$ denote the angle between v and w , $\theta(v, v^\perp)$ the angle between v and v^\perp . By the Cauchy-Schwarz inequality,

$$\begin{aligned} \langle v, w \rangle &= \left\langle v, \sum_{j=k+1}^d w_j u_j \right\rangle \\ &= \sum_{j=k+1}^d w_j \langle v, u_j \rangle \\ &\leq \left(\sum_{j=k+1}^d w_j^2 \right)^{1/2} \cdot \left(\sum_{j=k+1}^d v_j^2 \right)^{1/2} \\ &= \|w\| \cdot \|v^\perp\|. \end{aligned} \quad (12)$$

It follows that

$$\cos \theta(v, w) := \frac{\langle v, w \rangle}{\|v\| \|w\|} \leq \frac{\|v^\perp\|}{\|v\|} = \frac{\langle v, v^\perp \rangle}{\|v\| \|v^\perp\|} = \cos \theta(v, v^\perp). \quad (13)$$

Since the cosine function is monotonically decreasing on $[0, \pi]$, $\theta(v, w) \geq \theta(v, v^\perp)$ as claimed. \square

B Details of Experiment Setup

B.1 Applications and Datasets

The experiments are conducted with the following three applications.

1. **Image Classification.** We evaluate our framework on three widely used image datasets: MNIST [8], CIFAR-10, and CIFAR-100 [23]. For MNIST, we use LeNet5 [25], a lightweight convolutional network. For CIFAR-10, we adopt VGG11 [42], a deeper convolutional architecture. For CIFAR-100, we employ MobileNetV2 [40], a compact and efficient model ideal for large-scale image classification tasks.
2. **Text Classification.** We experiment with the 20 Newsgroups dataset [24], a benchmark dataset for multi-class text categorization. We adopt DistillBERT [41], a small transformer model suitable for resource-constrained devices.
3. **Human Activity Recognition.** We use the HAR [2] dataset, which contains time-series sensor data for different physical activities. We adopt the 1D version of ResNet18 [16], a modified ResNet architecture for processing 1D sequential data.

B.2 Baseline Methods

Below are the baseline methods that we compared in the experiments:

- **FedAvg** [33] is the classical synchronous algorithm where the server selects a subset of clients to conduct training in each round and synchronizes updates from these clients before aggregation.
- **FedProx** [28] is a synchronous method that addresses data heterogeneity by incorporating L2 regularization during local training to constrain the divergence between global and client models.
- **FedAdam** [38] is a synchronous algorithm that integrates Adam optimizer for the server. It adapts learning rates for each parameter using first- and second-moment estimates, improving convergence and accelerating training under data heterogeneity.
- **FedAsync** [50] is a fully-asynchronous framework that lets the server immediately aggregate the client updates into the global model upon receipt. It uses a weighting mechanism as in Equation 3 to account for the staleness of the updates.
- **FedBuff** [36] is a semi-asynchronous framework that introduces a buffered aggregation strategy. It maintains a buffer to collect client updates. Once the buffer is full, the server aggregates the client updates in the buffer and updates the global model.
- **CA²FL** [47] is another semi-asynchronous framework based on buffered aggregation. It caches the latest update from every client on the server and uses them to estimate the clients' contribution to the update of the current round and calibrate global updates.

B.3 Federated Learning Configuration

For reproducibility, we report the configurations in our experiments. The number of local training epochs $E = 5$. For the FedAvg algorithm, the number of sampled clients at each round is 10. The aggregation hyperparameters in Equation 4 are set to $\beta = 0.6$ and $\alpha = 0.5$, following the values used in prior work [50]. The learning rate for local training at all clients is 5×10^{-5} for the 20 Newsgroups dataset and 0.01 for the other datasets.

B.4 Derivation of Delay Distributions

Figure 9 presents the average communication and computation latency on Raspberry Pis scaled for the dataset and model configuration in our experiments. For 20 Newsgroups, the converted computational time is sufficiently long, making communication time negligible.

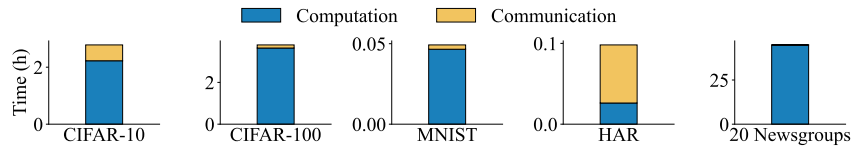


Figure 9: Average latency per round across clients.

Additional Delay Distributions. In Section 4.5, we present the performance of compared methods under additional delay distributions following physical deployments. The derivations of the additional delay distributions are as follows.

- **Lognormal distribution:** The parameters μ (mean) and σ (standard deviation) of the natural logarithm of delays are derived from the measurements on Raspberry Pis. Specifically, μ_R and σ_R represent the arithmetic mean and standard deviation of the measured delays for all rounds, respectively.

$$\sigma = \sqrt{\ln\left(\frac{\sigma_R^2}{\mu_R^2} + 1\right)}, \quad \mu = \ln(\mu_R) - \frac{\sigma^2}{2}$$

Then, the latency for each client is sampled from the lognormal distribution to capture skewed and heavy-tailed delays.

- **Half-normal distribution:** The mean and standard deviation of the delays (i.e., μ_R and σ_R) are calculated from the delay measurements on Raspberry Pis. Then, for each client, its latency is sampled from the half-normal distribution, ensuring non-negative values and a skewed distribution toward smaller delays.
- **Uniform distribution:** Client latency is sampled from a uniform distribution with bounds set between the 5th and 95th percentiles of the measurements from Raspberry Pis. This ensures outliers are excluded while covering the majority of the observed range.

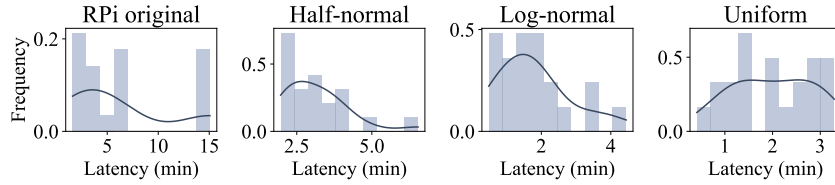


Figure 10: Delay patterns under different distributions: measurements from RPis show discrete peaks and high variability, half-normal and lognormal distributions have long tails, and uniform distribution assumes equal probability within a bounded range.

Figure 10 shows the simulated latency for 100 clients, each running CIFAR-100 with MobileNetV2 over 10,000 rounds.

C Connections with Other Areas

Asynchronous Stochastic Gradient Descent. Asynchronous stochastic gradient descent (SGD) is closely related to asynchronous federated learning and has provided theoretical and empirical foundations for scalable distributed training. Early studies analyzed error-runtime trade-offs, showing that incorporating stale gradients can alleviate system bottlenecks without significantly compromising accuracy [10]. Subsequent work refined convergence bounds based on maximum [43] or average [22] delay and demonstrated that asynchronous SGD can converge faster than traditional minibatch SGD [34]. To tackle challenges such as gradient staleness, communication delays, and convergence guarantees, various strategies have been proposed, such as filtering out outlier gradients [51, 7], adjusting update steps according to delay [35, 4], and approximating gradients to compensate for delayed information [61]. However, unlike federated learning, most asynchronous SGD formulations do not explicitly address non-i.i.d. data distributions or the strict data privacy constraints inherent in federated settings, which limits their direct applicability.

Continual Learning. There are works in continual learning [12, 5, 39, 29, 6] that leverage the idea of orthogonalization to project gradients onto non-conflicting subspaces across tasks. Continual learning aims to prevent catastrophic forgetting, where new knowledge overrides previously learned information when training a model on a sequence of tasks. It shares a common goal with asynchronous federated learning, which is to mitigate knowledge interference. Despite the similarities, the two fields follow distinct training paradigms. Continual learning typically processes tasks sequentially in a centralized setting. Methods can reuse data or access sample-level information (e.g., gradient) from previous tasks. In contrast, federated learning involves repeated rounds of training from distributed clients with data constraints. The model must integrate updates without knowing data or gradients from clients to preserve privacy. Therefore, the two fields require different optimization techniques and system designs.

D Adaptability to Dynamic Environments

The asynchrony and orthogonal calibration mechanisms not only accelerate training but also extend its applicability to more complex scenarios. These features make ORTHOFL suitable in dynamic federated learning environments. We discuss the following situations:

Dynamic Client Participation. In real-world federated learning applications, it is common for new clients to join the training process [37] or for previously unseen data with new tasks to appear over time [52, 53, 32, 9]. Scalability to new clients and tasks is essential for long-term performance. ORTHOFL is readily applicable to these settings. By orthogonal calibration on asynchronous updates, ORTHOFL mitigates the disruptive impact of newly joined clients, especially if the global model is well-trained and initial updates from newly joined clients are noisy or biased due to limited data or distribution shifts. Similarly, when new classes are introduced, ORTHOFL preserves knowledge of previously learned classes, reducing forgetting and performance degradation caused by sudden distribution shifts.

Failure Handling. Large-scale federated learning faces a high risk of client or system failures due to issues such as out-of-memory (OOM) errors during training, hardware malfunctions, or network interruptions [19, 14, 20, 48], particularly when training large models across many devices. Failure rates tend to increase with larger models and more clients, as the computational and communication demands scale up significantly. The ability to effectively handle these failures is critical for ensuring robust and reliable training in federated learning systems. The asynchronous nature of ORTHOFL makes it robust to such failures. When a client fails, training continues with updates from the remaining clients. A single node’s failure does not block global progress.

E Pseudo-code of ORTHOFL

Algorithm 1: ORTHOFL Framework

Input : Total number of updates T , local training epochs E , initial global model weights $W^{(0)}$.

Output : Global model weights $W^{(T+)}$.

Server execution:

Send $W^{(0)}$ to all available clients;

for $t = 1, \dots, T$ **do**

 Receive update from a client;

 Calculate delay $t - \tau$;

 Compute global weight shift: $\Delta W = W^{(t)} - W^{(\tau+)}$;

 Compute client weight change: $\Delta W_m = W_m^{(t)} - W_m^{(\tau+)}$;

 Orthogonalize each layer: $\Delta W^{l\perp} = \Delta W^l - \frac{\Delta W^l \cdot \Delta W_m^l}{\Delta W_m^l \cdot \Delta W_m^l} \Delta W_m^l$;

 Merge weights for client: $W_m^{(t+)} = W_m^{(t)} + \Delta W^{l\perp}$;

 Update global model: $W^{(t+)} = (1 - \beta_t)W^{(t)} + \beta_t W_m^{(t)}$;

 ClientUpdate($m, W_m^{(t+)}$)

return $W^{(T+)}$;

ClientUpdate(m, \tilde{W}):

Initialize local model: $W_m \leftarrow \tilde{W}$;

for $e = 1, \dots, E$ **do**

 Partition \mathbf{D}_m into mini-batches $\bigcup_{i=1}^{j_m} B_i^{(m)}$;

for $i = 1, \dots, j_m$ **do**

 Update local weights: $W_m \leftarrow W_m - \eta_c \nabla_{W_m} \mathcal{L}_m(W_m; B_i^{(m)})$;

return W_m to server;
